JACS
JOURNAL OF THE AMERICAN CHEMICAL SOCIETY

ARTICLE

pubs.acs.org/JACS

Reversible and Selective O_2 Chemisorption in a Porous Metal−Organic Host Material

Peter D. Southon,[†] David J. Price,[†] Pia K. Nielsen,[‡] Christine J. McKenzie,*[,‡] and Cameron J. Kepert*[,†]

[†]School of Chemistry, The University of Sydney, NSW 2006, Australia

[‡]Department of Physics and Chemistry, University of Southern Denmark, Campusvej 55, DK-5230 Odense M, Denmark

Supporting Information

ABSTRACT: The metal−organic host material $[\{Co^{III}_2(bpbp)(O_2)\}_2bdc](PF_6)_4$ (**1**·$2O_2$; $bpbp^-$ = 2,6-bis(*N*,*N*-bis(2-pyridylmethyl)aminomethyl)-4-*tert*-butylphenolato; bdc^{2-} = 1,4-benzenedicarboxylato) displays reversible chemisorptive desorption and resorption of dioxygen through conversion to the deoxygenated Co(II) form $[\{Co^{II}_2(bpbp)\}_2bdc](PF_6)_4$ (**1**). Single crystal X-ray diffraction analysis indicates that the host lattice **1**·$2O_2$, achieved through desorption of included water guests from the as-synthesized phase **1**·$2O_2$·$3H_2O$, consists of an ionic lattice containing discrete tetranuclear complexes, between which lie void regions that allow the migration of dioxygen and other guests. Powder X-ray diffraction analyses indicate that the host material retains crystallinity through the dioxygen desorption/chemisorption processes. Dioxygen chemisorption measurements on **1** show near-stoichiometric uptake of dioxygen at 5 mbar and 25 °C, and this capacity is largely retained at temperatures above 100 °C. Gas adsorption isotherms of major atmospheric gases on both **1** and **1**·$2O_2$ indicate the potential suitability of this material for air separation, with a O_2/N_2 selectivity factor of 38 at 1 atm. Comparison of oxygen binding in solution and in the solid state indicates a dramatic increase in binding affinity to the complex when it is incorporated in a porous solid.

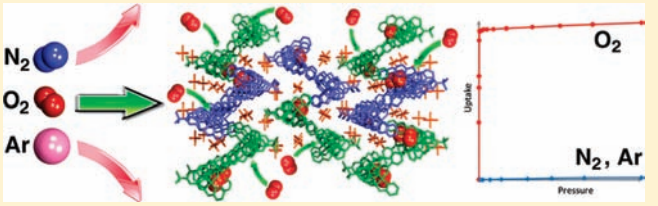

INTRODUCTION

Dioxygen, O_2, plays a central role in numerous large-scale processes, both biological and technological, making chemical manipulation of this molecule of fundamental importance. Biological systems have evolved proteins like hemoglobin, hemocyanin, and hemerythrin to perform O_2 separation and transportation through reversible chemisorptive O_2 binding. In contrast, all industrial processes to separate oxygen gas from air depend upon energy-intensive cryogenic distillation for large-scale production, or physisorption interaction with porous solids for smaller quantities.[1] Porous materials used in the separation of O_2 and N_2 by physisorption take advantage of differences in quadrupole moment (including various forms of zeolites A and X[1,2]) or molecular size (such as carbon-based molecular sieves[1,3]); however, these differences are quite small, leading to very similar physisorption enthalpies and thus limited selectivities. Conventional zeolites used for the portable upconcentration of O_2 from air for medical purposes typically achieve only a 3- to 4-fold selectivity, with N_2 adsorbed preferentially to O_2, leaving a residue of Ar.[2] A number of metal−organic frameworks have been reported recently that absorb O_2 much more readily than N_2 at temperatures below 100 K, ostensibly through physisorptive mechanisms;[4] however, the low temperatures required offer little improvement on cryogenic distillation. At the other end of the selectivity scale, the generation of highly anaerobic atmospheres (<1 ppm O_2) is commonly achieved through the use of certain metals and metal oxides, known as "getters". Here the local sites are irreversibly oxidized, providing the four electrons needed for O−O cleavage. Dioxygen cannot be recovered from getters, and they require chemical regeneration under an H_2 flow, producing water.[5,6] Lying at the interface between these selectivity extremes are biomimetic metallosupramolecular O_2 binding systems.[7−11] These systems exploit the different chemical reactivities of O_2 and N_2, specifically through coordination of the O_2 molecule to the metal ions and an accompanying one- or two- electron transfer, so that the adducts incorporate superoxo or peroxo ligands. This method achieves high chemical selectivity in a chemisorption process that is reversible without the need for chemical regeneration of the binding agent. While some iron complexes have been investigated,[12] complexes of cobalt have proved the most successful, the most frequently studied being mononuclear Co^{II} complexes with Schiff bases salen and fluomine.[7] These complexes have been shown to reversibly bind O_2 in the solid state, but long-term stability has been elusive due to a tendency for the metal ions to oxidize irreversibly to "met" forms (usually accompanied by the binding of a strongly bound ligand at the O_2 binding site) and to dimerize, e.g., formation of inactive M−O−M systems. Recent attempts to overcome these problems by incorporation into porous substrates[13−16] and synthesis of nanoparticles[17,18] have been reported. An alternative approach is the reversible O_2 binding to cyanide-coordinated Co^{II} centers, either within Co-based frameworks[19−21] or supported on a zeolite.[22] For the majority of these systems, the adsorption densities tend to be very

Received: March 22, 2011
Published: June 03, 2011

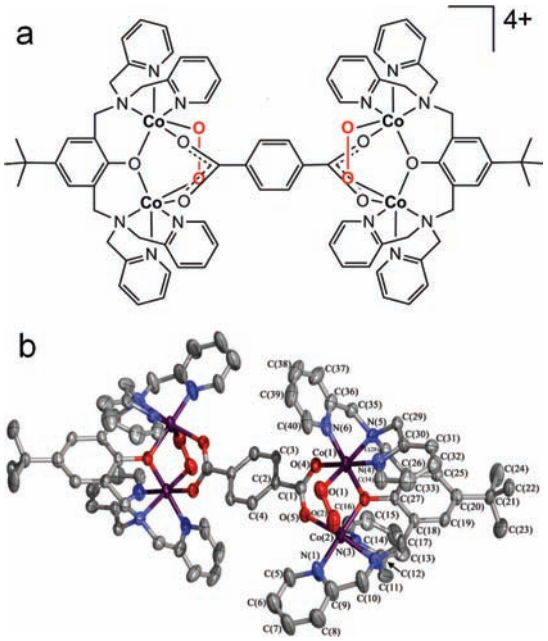

Figure 1. (a) Molecular structure of the cation in $1\cdot 2O_2$ and (b) crystal structure of $1\cdot 2O_2$ with atom labeling scheme (thermal ellipsoids shown at 50% probability, and H-atoms and counterions omitted for clarity).

low and the primary criteria of gas selectivity, reversibility, and stability are poorly characterized. These developments have arisen in parallel with rapid progress in gas binding in crystalline molecular materials such as metal−organic frameworks,[23] where intense recent focus in the generation of bare metal sites[24] has seen the achievement of high dihydrogen adsorption enthalpies for the purpose of hydrogen storage[25,26] and, most recently, in the chemisorptive binding of O_2 in the framework Cr_3(1,3,5-benzenetricarboxylate)$_2$.[27]

Suzuki and co-workers reported over 25 years ago that dicobalt complexes of phenoxo- and alkoxo-bridged dinucleating ligands show reversible O_2 binding in solution.[28−31] The main advantage of these systems compared to the mononuclear complexes discussed above is that inactivation by dimerization is prevented since both metal ions are involved in the binding of O_2. Analogously, the related ligand 2,6-bis(*N*,*N*-bis(2-pyridylmethyl)aminomethyl)-4-*tert*-butylphenolato (bpbp$^-$) forms dicobalt complexes that reversibly bind O_2 as a μ-peroxo ligand.[10] Monolayers of these complexes have been assembled on a gold surface, but the O_2 affinity was increased 1 million-fold in this process and thus the surface was not suitable for reversible O_2 binding.[32] Here, we investigate a tetranuclear relative $[\{Co^{III}_2(bpbp)(O_2)\}_2bdc](PF_6)_4$ ($1\cdot 2O_2$; bdc^{2-} = 1,4-benzenedicarboxylato), Figure 1 (a), and show that this host lattice exhibits solid-state O_2 binding that is both highly selective and fully reversible, the latter by mild thermal treatment with evacuation to give $[\{Co^{II}_2(bpbp)\}_2bdc](PF_6)_4$ (**1**). This material offers the prospect of use in O_2 enrichment from air by pressure and temperature-swing sorption technology and, conversely, the convenient generation of anaerobic atmospheres.

EXPERIMENTAL SECTION

Synthesis. Hbpbp was synthesized according to a method previously reported.[33] For the solution studies $[\{Co_2(O_2)(bpbp)\}_2bdc](ClO_4)_4$ was synthesized as reported previously[10] and dissolved in acetonitrile. For the synthesis of $1\cdot 2O_2\cdot 3H_2O$ (**1** = $[\{Co_2(bpbp)\}_2bdc](PF_6)_4$), solutions of Hbpbp (102 mg, 0.18 mmol in 25 mL of acetone) and $Co(NO_3)_2\cdot 6H_2O$ (103 mg, 0.32 mmol in 5 mL H_2O) were mixed to give a light brown solution. Sodium 1,4-benzenedicarboxylate (Na_2bdc; 19 mg, 0.10 mmol) in 3 mL H_2O was added, whereby the solution changed to a dark brown color. Ammonium hexafluorophosphate (59 mg, 0.36 mmol) dissolved in 2 mL H_2O was added to the reaction mixture. Slow evaporation in air at room temperature yielded black crystals overnight, which were isolated by filtration in yields of 80%-90%. The best fit for the elemental analyses was as a trihydrate, $1\cdot 2O_2\cdot 3H_2O$; Anal. Calcd. for $C_{80}H_{82}Co_4N_{12}O_{10}P_4F_{24}\cdot 3H_2O$: C, 42.87; H, 3.96; N, 7.50. Found for $1\cdot 2O_2\cdot 3H_2O$: C, 42.91; H, 3.72; N, 7.38.

Dioxygen Affinity in Solution. The affinity of the $[\{Co_2(bpbp)\}_2bdc]^{4+}$ species to O_2 in solution was determined by spectrophotometric measurements. A mixed O_2/Ar gas stream at various O_2 partial pressures was bubbled through *ca.* 0.1 mM solutions of the complex in acetonitrile at 40 °C. Absorption shoulders at 380 and 480 nm, absent in the deoxygenated form and which grow upon oxygenation, were monitored; from these was determined $P(O_2)_{50\%}$, the partial pressure of O_2 needed to oxygenate 50% of the complex. Further details are provided in the Supporting Information.

Single Crystal X-ray Diffraction (SCXRD). Single crystal X-ray diffraction data were collected at the Australian Synchrotron on the Protein Micro-Crystal and Small Molecule Diffraction Beamline 2 (PX2−3ID, λ = 0.652529 Å) equipped with an ADSC Q315r CCD detector and Oxford cryostream set at 100 K. A data set for the dehydrated sample, $1\cdot 2O_2$, was obtained consisting of 360 images of rotation angle 1° around the axis perpendicular to the beam, with 2 s exposure time, using the Blu-Ice GUI controller software.[34] Diffraction data analysis and reduction were performed within the XDS package.[35] Space group determination and SHELX file generation were performed within the program XPREP.[36] Structures were solved using direct methods using SHELXS-97[37] and refined using SHELXL-97 within the X-SEED program suite.[38] Non-hydrogen atoms were refined anisotropically with the exception of selected atoms of the two disordered PF_6^- counterions. Hydrogen atoms were included at calculated positions. The crystal structure has been deposited at the Cambridge Crystallographic Data Centre and allocated the deposition number CCDC 815290.

Synchrotron Powder X-ray Diffraction (S-PXRD). Powder X-ray diffraction patterns were measured on 1-BM at the Advanced Photon Source at Argonne National Laboratory (20.05 keV, 0.6183 Å) with a MAR-345 imaging plate detector. Samples of $1\cdot 2O_2\cdot 3H_2O$ were ground in mother liquor and loaded with solvent into glass capillaries. One capillary was sealed after loading, another sealed after evacuation at room temperature ($1\cdot 2O_2$), and a third sealed after evacuation at 95 °C (**1**). During measurement, the sample temperature was maintained at 200 K and diffraction patterns were collected with 36 s exposures. The raw images were processed using FIT2D.[39] The sample-to-detector distance and tilt of the image plate relative to the beam were refined using a LaB_6 standard.

The structure determined from SCXRD was used as the starting point for Rietveld refinements with EXPGUI and GSAS.[40] While the unit cells for $1\cdot 2O_2\cdot 3H_2O$ and $1\cdot 2O_2$ were refined successfully, the large unit cell, low symmetry, and large number of inequivalent atoms prevented refinement of atomic coordinates and displacement parameters. Attempts to fully index or refine the diffraction pattern of **1** were unsuccessful due to the very large number of overlapping reflections.

Thermogravimetry. Gravimetric characterization of guest desorption from $1\cdot 2O_2\cdot 3H_2O$ was performed using two methods. A conventional thermogravimetric measurement was carried out on a TA Instruments Hi-Res TGA 2950 Thermogravimetric Analyzer, ramping the sample temperature to 200° at 0.1 °C min^{-1} under flowing N_2. An equivalent measurement under vacuum used an IGA-002 gravimetric adsorption instrument (Hiden-Isochema, UK) in which the sample was evacuated at 5 mbar min^{-1} to a pressure of below 10^{-4} mbar, at which point it was assumed to have lost water but no appreciable O_2, and then heated to 150° at 0.1 °C min^{-1}.

Gas Adsorption. An IGA-002 gravimetric adsorption instrument (Hiden-Isochema, UK) was used to measure gas adsorption isotherms at 25 °C and at high temperatures. For the sorption isotherms on $\mathbf{1}\cdot 2O_2$ the solvated material $\mathbf{1}\cdot 2O_2\cdot 3H_2O$ was first evacuated to 10^{-5} mbar at room temperature to remove solvent. For the sorption isotherms on **1**, bound O_2 was removed by heating at high vacuum to 100 °C. Isotherms of O_2, N_2, Ar, and CO_2 (all 99.99%) were measured to 10 bar at 25.0 ± 0.1 °C. For the isotherms measured at 50−108 °C, the sample was heated by a furnace at a fixed temperature; convection effects led to a decline in sample temperature with increasing pressure of ca. 1 °C·bar^{-1}. The reproducibility of O_2 binding was demonstrated in a further experiment by cycling the sample five times between a desorption stage at 95 °C and a dosing stage at 10 mbar O_2. Low temperature adsorption isotherms were measured of N_2 (at 77 K) and Ar (at 77 and 87 K) on **1** and $\mathbf{1}\cdot 2O_2$ using a Micromeritics ASAP2020 instrument.

RESULTS AND DISCUSSION

Reversible O_2 Binding in Solution. Dark brown acetone, ethanol, methanol, and acetonitrile solutions of $[\{Co_2(O_2)(bpbp)\}_2bdc](ClO_4)_4$ change to a pale pink color upon heating or evacuation due to deoxygenation of the tetranuclear cation, a process that reverses rapidly on cooling or re-exposure to air. The partial pressure of O_2 needed to oxygenate 50% of the complex, $P(O_2)_{50\%}$, in acetonitrile solution at 40 °C was determined to be 15 mbar. This value is similar to the value recorded for related complexes[28,41] and prompted us to investigate this complex in the solid state.

Structure of $\mathbf{1}\cdot 2O_2$. The material was isolated in its oxygenated, hydrated form, $\mathbf{1}\cdot 2O_2\cdot 3H_2O$. Dried crystals of $\mathbf{1}\cdot 2O_2$ were analyzed by single crystal X-ray diffraction. In $\mathbf{1}\cdot 2O_2$, the tetranuclear complex cation $[\{Co_2(O_2)(bpbp)\}_2bdc]^{4+}$, which consists of two dinuclear Co^{III} centers bridged by bdc^{2-} (Figure 1), lies on an inversion center within the monoclinic space group $P2_1/n$ in a configuration similar to that seen in a previously reported perchlorate salt.[10] The O−O distance of 1.437(8) Å is consistent with assignment as a μ-peroxo bridge.[8,10,42] The two structurally inequivalent Co^{III} centers within each peroxo-bridged dinuclear unit are each coordinated by two pyridyl and one amine nitrogen donor atoms from the $bpbp^-$ ligand, one μ-peroxo-O atom and one carboxylate O atom from the bdc^{2-} ligand. These centers have subtly different coordination configurations. For Co(1), the $Co(1)-O(1)_{peroxo}$ bond lies trans to the $Co(1)-N(5)_{amine}$ bond, where the latter is elongated slightly (2.021(5) Å) compared to the two pyridyl bonds, $Co(1)-N_{py}(av)$ = 1.93(1) Å. The $Co(1)-O(1)_{peroxo}$ bond (1.851(4) Å) is significantly shorter than the $Co(1)-O(3)_{bpbp}$ and $Co(1)-O(4)_{bdc}$ bonds of 1.900(4) and 1.939(4) Å, respectively. The major stereochemical difference between Co(1) and Co(2) is that the $Co(2)-N(3)_{py}$ bond lies trans to the $Co(2)-O(2)_{peroxo}$ bond of 2.017(6) and 1.890(6) Å, respectively. The remaining Co(2)-donor bond lengths are 1.918(6) ($N(1)_{py}$), 1.964(5) ($N(2)_{amine}$), 1.890(6) ($O(2)_{peroxo}$), 1.915(4) ($O(3)_{bpbp}$) and 1.921(4) Å ($O(5)_{bdc}$).

In the solid state packing of $\mathbf{1}\cdot 2O_2$ edge-to-face interactions exist between one of the pyridyl rings of the $bpbp^-$ ligand on one cation and the bdc^{2-} ligand on an adjacent cation, with a py-H···$centroid_{bdc}$ distance of ca. 3.06 Å. This results in chains of cations packing parallel to the *a*-axis direction, as depicted in Figure 2(a). These chains stack in zigzag layers running parallel to the *b*-axis direction, shown in Figure 2(b). These layers stack perpendicular to the *c*-axis direction, alternating with PF_6^- counteranions. Between these zigzag layers lie regions of guest-accessible pore volume. The

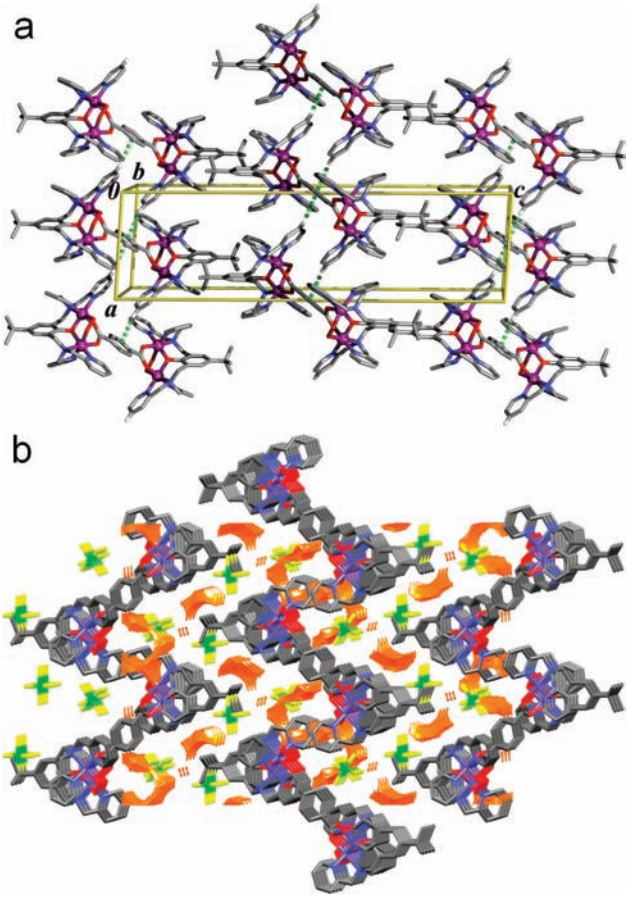

Figure 2. Crystal packing of $\mathbf{1}\cdot 2O_2$ showing (a) edge-to-face H···π interactions producing chains of cations parallel to the *a*-axis direction and (b) packing of these chains viewed along the *a*-axis direction. Semitransparent orange contours show the void regions. Secondary orientations of the disordered PF_6^- counterions are omitted for clarity.

similarity between the unit cell parameters and simulated PXRD pattern for this structure and those determined for $\mathbf{1}\cdot 2O_2$ by S-PXRD, and dissimilarity with those for $\mathbf{1}\cdot 2O_2\cdot 3H_2O$ (see Figure 3 and Table 1), confirm that the crystal structure was that of $\mathbf{1}\cdot 2O_2$. The calculated[43] solvent-accessible void volume is 13.5% of crystal volume when using a probe diameter of 2.4 Å. If the probe diameter is increased to 3.4 Å, comparable with the kinetic diameter of O_2 (3.5 Å),[44] then the calculated void space is zero. For comparison, the kinetic diameter of water is 2.7 Å.[44]

Desolvation and Deoxygenation of $\mathbf{1}\cdot 2O_2\cdot 3H_2O$. Thermogravimetric analyses, measured both under vacuum and flowing N_2, show two stages of mass loss, attributed to the removal of water and O_2, respectively. Full data are provided in the Supporting Information, SI. The loss of water and surface solvent (approx 3−4% of the desolvated mass) was completed during evacuation at 25 °C, and was observed at 25−50 °C under flowing N_2. The powder X-ray diffraction pattern of the desolvated material varies only slightly from that of the solvated material (Figure 3). Unit cell parameters determined from the fitting of these patterns (see Table 1) indicate a slight contraction along each of the monoclinic axes and widening of the monoclinic cell angle upon desorption of the unbound water guests. Together, these changes constitute only a slight contraction of the unit cell, amounting to a 3.5% reduction in volume.

The removal of O_2 (calculated 2.93%, measured 2.92% of the desolvated mass) was observed by thermogravimetry in the range of 100−130 °C under N_2 flow and 50−100 °C under dynamic vacuum (Figures S1 and S2 of the SI). As with solutions of the complex, the solid changes from dark brown to a dark pink color upon dioxygen release, which is reversible on reintroduction of O_2. The powder diffraction pattern of **1** (Figure 3) demonstrates that the material retains crystallinity, but upon deoxygenation undergoes a modest structural change. The shift in the lowest angle peak, ⟨002⟩, suggests an increase in the *c* parameter from 36.835 to ca. 40.8 Å, but thus far we have been unsuccessful both in obtaining single crystals of the deoxygenated form and in indexing the powder pattern.

Sorption of Gases into 1. Exposure of **1** to very low pressures of O_2 (5 mbar) at 25 °C leads to a mass uptake of 2.80 wt %. This is the equivalent of 1.86 mol of O_2 per mole of complex, or 93% of the theoretical chemisorptive capacity. It is not yet determined whether the marginally substoichiometric uptake is due to incomplete initial removal of O_2 or incomplete binding upon exposure to O_2. On a volumetric basis, the equivalent of 1290 mol of O_2 is adsorbed per m^3, corresponding to 32 times the concentration of O_2 in a 1 atm gaseous sample of pure O_2, or approximately 160 times that in air. When dosing O_2 to pressures below 5 mbar, the kinetics of adsorption are quite slow, making precise measurements difficult; however, the value of $P(O_2)_{50\%}$ estimated from the isotherm at 25 °C is no greater than 0.5 mbar. The uptake is relatively rapid when dosing with O_2 at pressures above 5 mbar; fitting with the linear driving force model (see SI) yields a rate coefficient of 5.5 min. The sorption isotherm to 1 bar is shown in Figure 4, and to 10 bar in Figure S3 of the SI. Beyond 5 mbar, the uptake increases slightly with increasing pressure; this contribution is completely reversible without hysteresis and is attributed to physisorption. The chemisorbed component remains upon decreasing the pressure to below 1 mbar at 25 °C but is readily desorbed at elevated temperatures (see below). We have carried out five desorption-chemisorption cycles without observing any degradation of capacity (see SI).

Sorption isotherms for other atmospheric gases on **1** were also measured at 25 °C and are plotted in Figure 4. Uptakes of N_2 and Ar are much lower, lying well below 0.1 mol/mol at 10 bar (see SI). In contrast, significant CO_2 uptakes, of 0.50 and 1.74 mol/mol, occur at 1 and 10 bar, respectively. The shape and reversibility of these isotherms indicate physisorption on the surface rather than chemisorption. The higher uptake of CO_2 is consistent with the much greater interaction potential of CO_2 with pore surfaces.

Sorption of Gases into 1·2O₂. To determine the physisorption behavior of the chemisorbed host, which is relevant in the assessment of the gas physisorption selectivity for air separation, gas isotherms for individual gases were measured on samples of the O_2-chemisorbed host **1**·$2O_2$. Isotherms to 1 bar are plotted in Figure 5, while the full isotherms to 10 bar are presented in the SI. As expected, the isotherm of O_2 on **1**·$2O_2$ matches the physisorption-only component of the isotherm of O_2 for **1** without the large chemisorption step below 5 mbar. Interestingly, **1**·$2O_2$ takes up larger amounts of CO_2 and N_2 than does **1**; uptakes of CO_2 and N_2 at 10 bar were 5.67 and 0.42 mol/mol, respectively. This indicates that the structure of **1**·$2O_2$ is significantly more open than that of **1**, with the open pore regions seen in the crystal structure of **1**·$2O_2$ likely to be partially obstructed and/or lost in the apohost **1**.

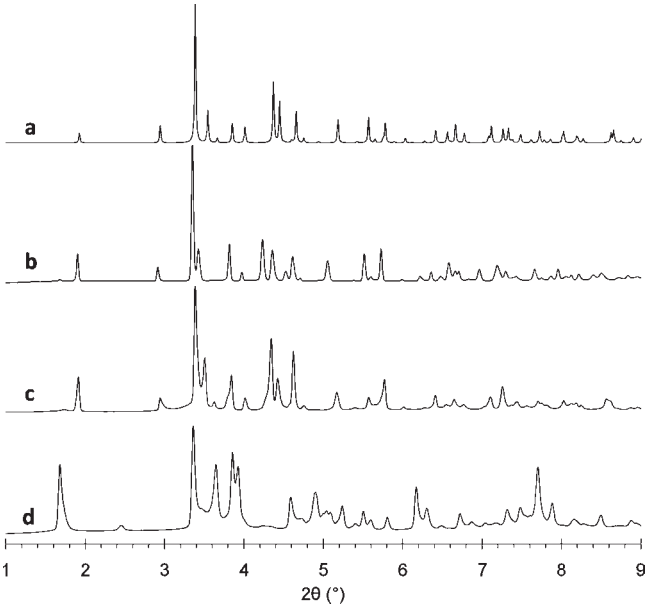

Figure 3. S-PXRD for (a) **1**·$2O_2$, simulated from the SCXRD structure, (b) **1**·$2O_2$·$3H_2O$, (c) **1**·$2O_2$, sample evacuated at room temperature, and (d) **1**, sample evacuated and heated to 95 °C.

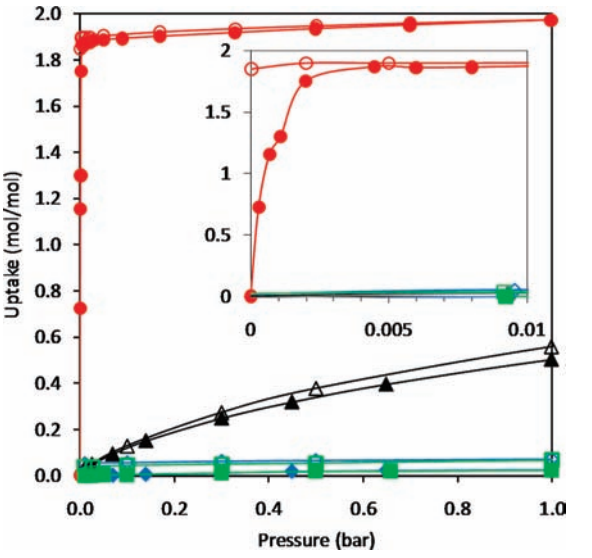

Figure 4. Gas sorption isotherms for O_2 (red ●), CO_2 (black ▲), N_2 (blue ♦), and Ar (green ■) on **1** at 25 °C. Unfilled data points were measured during desorption after a maximum pressure of 10 bar. Inset: expansion of the low pressure region.

Table 1. Unit Cell Parameters Determined from SCXRD and S-PXRD

material	method	*T* (K)	*a* (Å)	*b* (Å)	*c* (Å)	*β* (°)	V (Å^3)
1·$2O_2$	SCXRD	100(2)	10.225(2)	12.729(3)	36.869(7)	93.69	4788.7(16)
1·$2O_2$·$3H_2O$	S-PXRD	200	10.4733(12)	12.7866(15)	37.086(5)	94.997(10)	4947.6(7)
1·$2O_2$	S-PXRD	200	10.289(2)	12.631(2)	36.835(8)	93.75(2)	4776.6(12)

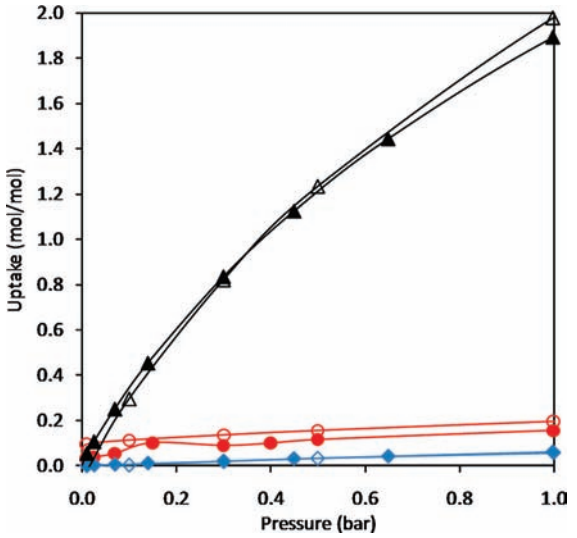

Figure 5. Gas adsorption isotherms to 1 bar for O_2 (red ●), CO_2 (black ▲) and N_2 (blue ♦) on $\mathbf{1}\cdot 2O_2$ at 25 °C. Unfilled data points were measured during desorption after a maximum pressure of 10 bar.

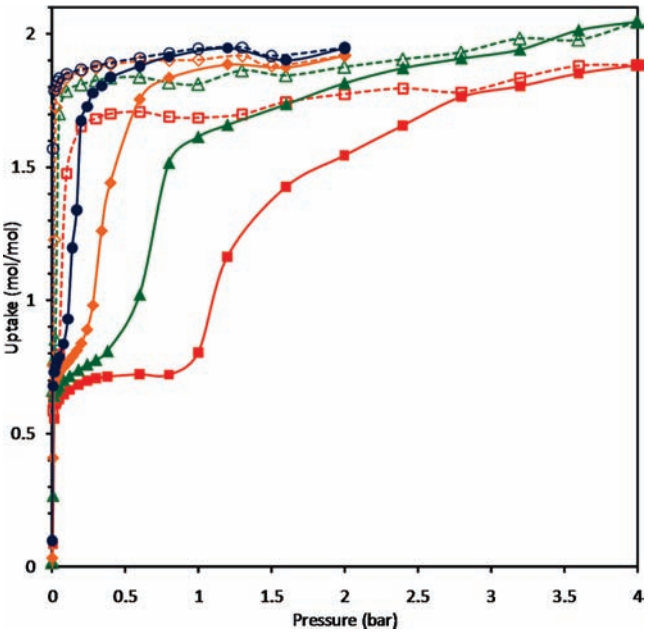

Figure 6. Gas sorption isotherms for O_2 on **1** at 80 °C (blue ●), 90 °C (orange ♦), 99 °C (green ▲), and 108 °C (red ■). Unfilled data points were measured during desorption. Isotherms measured at 50 and 70 °C are omitted for clarity, and are given in the SI.

These isotherms can be used to approximate gas separation selectivity based on the assumption that the adsorption of mixed gases will be essentially noncompeting at low loadings—an approximation that is reasonable given that the gas isotherms for $\mathbf{1}\cdot 2O_2$ follow the Langmuir model.[45] On the basis of these data, upon exposure of **1** to 1 bar of dry air (78% N_2, 21% O_2, 0.9% Ar, 0.04% CO_2) this apohost material will rapidly convert to $\mathbf{1}\cdot 2O_2$ and physisorb small quantities of all four gases to give a calculated composition of all removable physisorbed and chemisorbed species of 97% O_2, 2.5% N_2, 0.1% CO_2 and 0.02% Ar. This can also be expressed as a O_2/N_2 selectivity factor of 38; this is substantially higher than the 3- to 4-fold enrichment achieved typically with physisorption media,[1−3] and higher than the factor of 22 reported for Cr_3(1,3,5-benzenetricarboxylate)$_2$ at 25 °C.[27]

Low Temperature Gas Adsorption. Dinitrogen and argon adsorption isotherms measured at 77 K showed negligible uptake for both **1** and $\mathbf{1}\cdot 2O_2$ (Figure S8 of the SI), less than 0.12 mmol/g (<0.25 mol/mol), equivalent to surface area well below 5 m^2/g. The shape and magnitude of the isotherms are consistent with adsorption on the surface of the crystallites and absence of accessible micropore volume. However, Ar adsorption isotherms at 87 K showed somewhat higher uptake, approaching 1 mmol/g (2 mol/mol) near saturation pressure. We attribute the difference over 10 K to thermally activated diffusion through the narrow pore windows, an effect that can arise due both to the increased thermal energies of the guests and from a thermally induced opening of narrow pore windows. We can also attribute to this effect the higher uptakes of O_2 and CO_2 at higher temperatures.

High Temperature Gas Sorption. With the expectation that dramatically increased gas sorption selectivities may be achievable at higher temperatures due to a pronounced decrease in physisorptive uptake, O_2 isotherms were measured in the temperature range 50−108 °C to determine the extent of chemi- and physisorption (see Figure 6). At these temperatures, O_2 desorption is readily achieved on the down swing, leading to a closing of the isotherm loops. The loops display considerable hysteresis, characteristic of chemisorption, and show clearly that the chemisorption process is divided into two stages: approximately 0.6 − 0.8 mol/mol is taken up at very low pressure (below 20 mbar), while a further 1.0−1.2 mol/mol is adsorbed at higher pressures. With increasing temperature, the pressures at which these two stages occur also increase. The desorption curve is also affected by temperature, and at higher temperatures also shows two stages. Low pressures are still required to remove the bound O_2 at the temperatures investigated; at 108 °C the most loosely bound O_2 can be removed below 40 mbar, and the more tightly bound O_2 requires pressures below 5 mbar. The existence of the step in the isotherms appears most likely to be a solid state effect resulting from a structural arrangement in which some of the dinuclear binding sites have a local chemical environment more favorable for O_2 binding, or are more accessible through the pore windows. An alternative explanation for this behavior might lie in an allosteric inhibition of the O_2 binding, i.e., O_2 binding at one end of the molecule lowers the affinity for O_2 binding at the other end.

The high temperature sorption isotherms were used to construct a Clausius−Clapeyron plot (see SI for details). The calculated enthalpies of binding were −55 kJ/mol for the first stage, and −88 kJ/mol for the second stage. These values are comparable with values of −56 to −80 kJ/mol reported for O_2 binding to Co complexes in the solid state.[46] The increase in calculated binding energy between the first and second stage is unexpected, and, if real (and not, for example, an artifact arising from nonequilibrium effects associated with the broad hysteresis in the second sorption step), may arise due to a crystal packing contribution at higher O_2 loading, as is expected given the observed change in the S-PXRD pattern upon O_2 sorption/desorption. This plot also allows us to directly extrapolate a value of $P(O_2)_{50\%}$ in the solid state at 40 °C. The calculated value of 2 mbar is substantially lower than the measured value of 15 mbar in solution, a difference that supports the view that the O_2 binding sites are not significantly occluded in the solid state. We attribute this difference to the stabilization of the deoxygenated complex in solution by metal-solvent interactions, an effect not present in the solid state.

CONCLUSIONS

Porous molecular lattices containing chemically selective binding sites can reversibly bind large quantities of oxygen gas in the solid state with very high selectivity. The oxygen-binding affinity has been measured in solution, and this property is clearly retained in the solid state. The O_2/N_2 selectivity factor of 38 is the highest reported value to our knowledge for reversible binding at ambient temperatures, and the adsorption characteristics of other atmospheric gases have also been characterized. The dioxygen capacity is largely retained at temperatures above 100 °C, and preliminary cycling experiments show no sign of host lattice degradation. Such materials represent a significant improvement compared to N_2/O_2 concentrating ratios in zeolite physisorption systems, and have considerable potential for application in dioxygen separation and purification from air, for use in anaerobic packaging, oxygen sensing, and medical devices.

ASSOCIATED CONTENT

Supporting Information. Full details on O_2 affinity measurements in solution, crystallographic refinement details, thermogravimetric data, gas adsorption data to 10 bar, details on sorption/desorption cycles, low temperature isotherms, high temperature isotherms and the calculation of enthalpies, Raman and visible-NIR spectra, and the Crystallographic Information File for $\mathbf{1}\cdot 2O_2$. This material is available free of charge via the Internet at http://pubs.acs.org.

AUTHOR INFORMATION

Corresponding Author
chk@ifk.sdu.dk; c.kepert@chem.usyd.edu.au

ACKNOWLEDGMENT

This work was supported by two Australian Research Council Discovery Project Grants (DP0985611 and DP0664834). We thank Dr. Frank Johansson for carrying out solution spectrophotometric measurements and O_2 affinity calculations. Single crystal X-ray diffraction was undertaken on the Micro Crystallography beamline at the Australian Synchrotron, Victoria, Australia. Work done at Argonne National Laboratory and use of the Advanced Photon Source was supported by the U.S. Department of Energy, Office of Science, Basic Energy Sciences, under Contract No. DE-AC02-06CH11357, and travel funding was provided by the Australian Synchrotron Research Program, which is funded by the Commonwealth of Australia under the Major National Research Facilities Program. We thank Dr. Gregory Halder and Dr. Karena Chapman for beamline support. We acknowledge the Danish Research Council for Natural Sciences and The University of Sydney for a Visiting Professorship to C.J.M.

REFERENCES

(1) Gaffney, T. R. *Curr. Opin. Solid State Mater. Sci.* **1996**, *1*, 69.
(2) Sircar, S.; Rao, M. B.; Golden, T. C. In *Adsorption and Its Applications in Industry and Environmental Protection, Vol I: Applications in Industry*; Elsevier Science Publ B V: Amsterdam, 1999; Vol. 120, p 395.
(3) Ismail, A. F.; David, L. I. B. *J. Membr. Sci.* **2001**, *193*, 1.
(4) Li, J.-R.; Kuppler, R. J.; Zhou, H.-C. *Chem. Soc. Rev.* **2009**, *38*, 1477.
(5) Giorgi, T. A.; Ferrario, B.; Storey, B. *J. Vac. Sci. Technol. A-Vac. Surf. Films* **1985**, *3*, 417.
(6) Holtz, R. L.; Provenzano, V.; Imam, M. A. *Nanostruct. Mater.* **1996**, *7*, 259.
(7) Li, G. Q.; Govind, R. *Ind. Eng. Chem. Res.* **1994**, *33*, 755.
(8) Ghiladi, M.; Gomez, J. T.; Hazell, A.; Kofod, P.; Lumtscher, J.; McKenzie, C. J. *Dalton Trans.* **2003**, 1320.
(9) Larsen, P. L.; Parolin, T. J.; Powell, D. R.; Hendrich, M. P.; Borovik, A. S. *Angew. Chem., Int. Ed.* **2003**, *42*, 85.
(10) Johansson, F. B.; Bond, A. D.; McKenzie, C. J. *Inorg. Chem.* **2007**, *46*, 2224.
(11) Carlton, L.; Mokoena, L. V.; Fernandes, M. A. *Inorg. Chem.* **2008**, *47*, 8696.
(12) MacBeth, C. E.; Golombek, A. P.; Young, V. G.; Yang, C.; Kuczera, K.; Hendrich, M. P.; Borovik, A. S. *Science* **2000**, *289*, 938.
(13) Hutson, N. D.; Yang, R. T. *Ind. Eng. Chem. Res.* **2000**, *39*, 2252.
(14) Sharma, A. C.; Borovik, A. S. *J. Am. Chem. Soc.* **2000**, *122*, 8946.
(15) Corriu, R. J. P.; Lancelle-Beltran, E.; Mehdi, A.; Reye, C.; Brandes, S.; Guilard, R. *J. Mater. Chem.* **2002**, *12*, 1355.
(16) Welbes, L. L.; Borovik, A. S. *Acc. Chem. Res.* **2005**, *38*, 765.
(17) Johnson, C.; Long, B.; Nguyen, J. G.; Day, V. W.; Borovik, A. S.; Subramaniam, B.; Guzman, J. *J. Phys. Chem. C* **2008**, *112*, 12272.
(18) Johnson, C.; Ottiger, S.; Pini, R.; Gorman, E. A.; Nguyen, J. G.; Munson, E. J.; Mazzotti, M.; Borovik, A. S.; Subramaniam, B. *AlChE J.* **2009**, *55*, 1040.
(19) Ramprasad, D.; Pez, G. P.; Toby, B. H.; Markley, T. J.; Pearlstein, R. M. *J. Am. Chem. Soc.* **1995**, *117*, 10694.
(20) Ramprasad, D.; Markley, T. J.; Pez, G. P. *J. Mol. Catal. A: Chem.* **1997**, *117*, 273.
(21) Meier, I. K.; Pearlstein, R. M.; Ramprasad, D.; Pez, G. P. *Inorg. Chem.* **1997**, *36*, 1707.
(22) Taylor, R. J.; Drago, R. S.; Hage, J. P. *Inorg. Chem.* **2002**, *31*, 253.
(23) Kitaura, R.; Kitagawa, S.; Kubota, Y.; Kobayashi, T. C.; Kindo, K.; Mita, Y.; Matsuo, A.; Kobayashi, M.; Chang, H. C.; Ozawa, T. C.; Suzuki, M.; Sakata, M.; Takata, M. *Science* **2002**, *298*, 2358.
(24) Kitagawa, S.; Noro, S.; Nakamura, T. *Chem. Commun.* **2006**, 701.
(25) Dinca, M.; Long, J. R. *Angew. Chem., Int. Ed.* **2008**, *47*, 6766.
(26) Peterson, V. K.; Liu, Y.; Brown, C. M.; Kepert, C. J. *J. Am. Chem. Soc.* **2006**, *128*, 15578.
(27) Murray, L. J.; Dinca, M.; Yano, J.; Chavan, S.; Bordiga, S.; Brown, C. M.; Long, J. R. *J. Am. Chem. Soc.* **2010**, *132*, 7856.
(28) Sugimoto, H.; Nagayama, T.; Maruyama, S.; Fujinami, S.; Yasuda, Y.; Suzuki, M.; Uehara, A. *Bull. Chem. Soc. Jpn.* **1998**, *71*, 2267.
(29) Suzuki, M.; Kanatomi, H.; Murase, I. *Chem. Lett.* **1981**, *12*, 1745.
(30) Suzuki, M.; Ueda, I.; Kanatomi, H.; Murase, I. *Chem. Lett.* **1983**, *12*, 185.
(31) Suzuki, M.; Kanatomi, H.; Murase, I. *Bull. Chem. Soc. Jpn.* **1984**, *57*, 36.
(32) Wackerbarth, H.; Larsen, F. B.; Hansen, A. G.; McKenzie, C. J.; Ulstrup, J. *Dalton Trans.* **2006**, 3438.
(33) Ghiladi, M.; McKenzie, C. J.; Meier, A.; Powell, A. K.; Ulstrup, J.; Wocadlo, S. *J. Chem. Soc., Dalton Trans.* **1997**, 4011.
(34) McPhillips, T. M.; McPhillips, S. E.; Chiu, H.-J.; Cohen, A. E.; Deacon, A. M.; Ellis, P. J.; Garman, E.; Gonzalez, A.; Sauter, N. K.; Phizackerley, R. P.; Soltis, S. M.; Kuhn, P. *J. Synchrotron Rad.* **2002**, *9*, 401.
(35) Kabsch, W. *J. Appl. Crystallogr.* **1993**, *26*, 795.
(36) XPREP version 6.14, Reciprocal space exploration tool, Bruker Analytical X-ray Instruments Inc., 2003.
(37) Sheldrick, G. M. SHELXTL 97, Program for crystal structure solution and refinement; University of Göttingen: Göttingen, Germany, 1997.
(38) Barbour, L. J. *X-SEED: Crystallographic Interface Program*; University of Missouri, Missouri: Columbia, USA, 1999.
(39) Hammersley, A. P. FIT2D: An Introduction and Overview; ESRF Internal Report ESRF97HA02T, 1997.

(40) Toby, B. H. *J. Appl. Crystallogr.* **2001**, *34*, 210.
(41) Kayatani, T.; Hayashi, Y.; Suzuki, M.; Uehara, A. *Bull. Chem. Soc. Jpn.* **1994**, *67*, 2980.
(42) Bigoli, F.; Lanfranchi, M.; Leporati, E.; Pellinghelli, M. A. *Cryst. Struct. Commun.* **1981**, *10*, 1445.
(43) Spek, A. L. PLATON, A *Multipurpose Crystallographic Tool*, Utrecht University, Utrecht, The Netherlands, 2010.
(44) Breck, D. W. *Zeolite Molecular Sieves*; Wiley: New York, 1974.
(45) Rouquerol, F.; Rouquerol, J.; Sing, K. *Absorption by Powders and Porous Solids*; Academic Press: London, 1998.
(46) Niederhoffer, E. C.; Timmons, J. H.; Martell, A. E. *Chem. Rev.* **1984**, *84*, 137.